FEBS openbio

FEBS PRESS
science publishing by scientists

Oxygen activation in NO synthases: evidence for a direct role of the substrate

Albane Brunel[1], Jérôme Lang[2], Manon Couture[2], Jean-Luc Boucher[3], Pierre Dorlet[1] and Jérôme Santolini[1]

1 Laboratoire Stress Oxydant et Détoxication, Institute for Integrative Biology of the Cell (I2BC), CEA, CNRS, Université Paris-Saclay, Gif-sur-Yvette Cedex, France
2 Département de biochimie, de microbiologie et de bio-informatique, and PROTEO, Pavillon Charles-Eugène Marchand, Université Laval, Québec, Canada
3 UMR 8601 CNRS-University Paris Descartes, Paris, France

Keywords
kinetics; mechanism; nitric oxide synthase; oxygen activation; resonance Raman spectroscopy

Correspondence
J. Santolini, Laboratoire Stress Oxydant et Détoxication, Institute for Integrative Biology of the Cell (I2BC), iBiTec-S, CEA Saclay, 91191 Gif-sur-Yvette Cedex, France
Fax: +33 1 69 08 87 17
Tel: +33 1 69 08 53 63
E-mail: jerome.santolini@cea.fr

(Received 26 October 2015, revised 15 December 2015, accepted 13 January 2016)

doi:10.1002/2211-5463.12036

Nitric oxide (NO) and the other reactive nitrogen species (RNOS) play crucial patho-physiological roles at the interface of oxidative stress and signalling processes. In mammals, the NO synthases (NOSs) are the source of these reactive nitrogen species, and so to understand the precise biological role of RNOS and NO requires elucidation of the molecular functioning of NOS. Oxygen activation, which is at the core of NOS catalysis, involves a sophisticated sequence of electron and proton transfers. While electron transfer in NOS has received much attention, the proton transfer processes has been scarcely investigated. Here, we report an original approach that combines fast-kinetic techniques coupled to resonance Raman spectroscopy with the use of synthetic analogues of NOS substrate. We characterise Fe^{II}-O_2 reaction intermediates in the presence of L-arginine (Arg), alkyl- and aryl-guanidines. The presence of new reaction intermediates, such as ferric haem-peroxide, that was formerly postulated, was tracked by analysing the oxygen activation reaction at different times and with different excitation wavelengths. Our results suggest that Arg is not a proton donor, but indirectly intervenes in oxygen activation mechanism by modulating the distal H-bond network and, in particular, by tuning the position and the role of the distal water molecule. This report supports a catalytic model with two proton transfers in step 1 (Arg hydroxylation) but only one proton transfer in step 2 (N^{ω}-hydroxy-L-arginine oxidation).

Nitric oxide (NO) synthases were first characterised in mammals in the early 1990s as the source of NO in mammalian cells. Constitutive NO synthases (NOSs) are involved in signalling processes such as blood pressure regulation and angiogenesis (eNOS) [1] or learning process, synaptic plasticity and neurotransmission (nNOS) [2]. The inducible NOS (iNOS) is recruited for nonspecific immune response against tumours, viruses or bacteria [3]. On the other hand, NOSs have been increasingly associated with the development of several pathologies including cardiovascular, inflammatory and neurodegenerative diseases, diabetes and cancers [4–7].

Abbreviations
4-CF_3-phgua, 4-trifluoromethyl-phenyl-guanidine; 4-Clphgua, 4-chlorophenyl-guanidine; 4-Fphgua, 4-fluorophenyl-guanidine; 4-MeOphgua, 4-methoxyphenyl-guanidine; Arg, L-arginine; BH_2, dihydrobiopterin; BH_4, tetrahydrobiopterin, (6R)-5,6,7,8-tetrahydro-L-biopterin; Cpd I, Compound I in chloroperoxidase, cytochrome P450 and catalase catalytic cyle; iNOS, inducible nitric oxide synthase; NO, nitric oxide; NOHA, N^{ω}-hydroxy-L-arginine; NOS, nitric oxide synthase; NOSoxy, oxygenase domain of NOS; NOSred, reductase domain of NOS; Pentylgua, *n*-pentyl-guanidine; RR, resonance Raman.

Despite a broad range of biological activities, mammalian NOSs share a similar 3D structure and a common catalytic mechanism. NOSs synthesise NO in two stages [8]: the first haem-based oxidation converts L-arginine (Arg) to a stable intermediate, N^{ω}-hydroxy-L-arginine (NOHA), and the second converts NOHA to L-citrulline and NO [9,10]. Mammalian NOSs are homodimers that contain an N-terminal oxygenase domain (NOSoxy) and a C-terminal reductase domain (NOSred). Electron transfer between the two domains is regulated by a Calmoduline-binding interface. NOSoxy binds Arg, the haem cofactor and the redox-active cofactor tetrahydrobiopterin (BH_4). NOSred is similar to P450 reductase and thus contains an NADP(H)- and FAD-binding flavodoxin-reductase module and a flavodoxin-like FMN-binding domain [8,11,12]. Due to the high biomedical importance of mNOSs, their molecular mechanism has attracted tremendous interest. The first O_2 activation step (Step 1) is similar but distinct from that of the cytochromes P450 (Fig. 1) [13]: NOS catalysis begins with the reduction in the high-spin ferric haem (Fe^{III}) to ferrous haem (Fe^{II}) by NOSred (with electrons originating from NADPH). Subsequent O_2 binding forms the ferric superoxo-haem (Fe^{III}-OO°) [14], which is further reduced by BH_4 and protonated to form the ferric hydroperoxo-haem (Fe^{III}-OOH) [15–18]. The hydroperoxo-haem is thought to collapse to a Compound I intermediate (Cpd I: $Fe^{IV}(O)$-$\pi^{\bullet+}$), which then hydroxylates Arg. The $BH_4^{\bullet+}$ radical is then re-reduced by NOSred [19]. In the second stage (Step 2), product formation requires only one electron, whereas oxygen activation still requires two electrons. The hydroperoxo intermediate, once formed, directly reacts with NOHA to eventually produce L-citrulline and NO. In this stage, the second electron needed for oxygen activation may be shuttled back to the $BH_4^{\bullet+}$ radical from a transient redox intermediate, which may be nitroxyl (NO^-) [20].

However, this sequence remains essentially hypothetical. The only reaction intermediate that has been identified so far, besides the oxygenated complex, is the haem-peroxide species, and only through cryo-reduction approaches [21,22] that do not mimic catalytic conditions. There is also no clear understanding of the reason of the coexistence of two distinct mechanisms for the two catalytic steps: if the first step of O_2 activation is similar to what has been proposed for cytochromes P450, the second step is specific to NOS. Many research programmes have investigated two major specificities of NOS catalysis, which is the electron transfer by the BH_4 cofactor [23–25] and the push effect of the proximal ligand [26–28]. However, only scarce attention has been devoted to the proton transfer process (nature of the proton donor, sequence and pathway of proton transfer). Proton transfer is also at

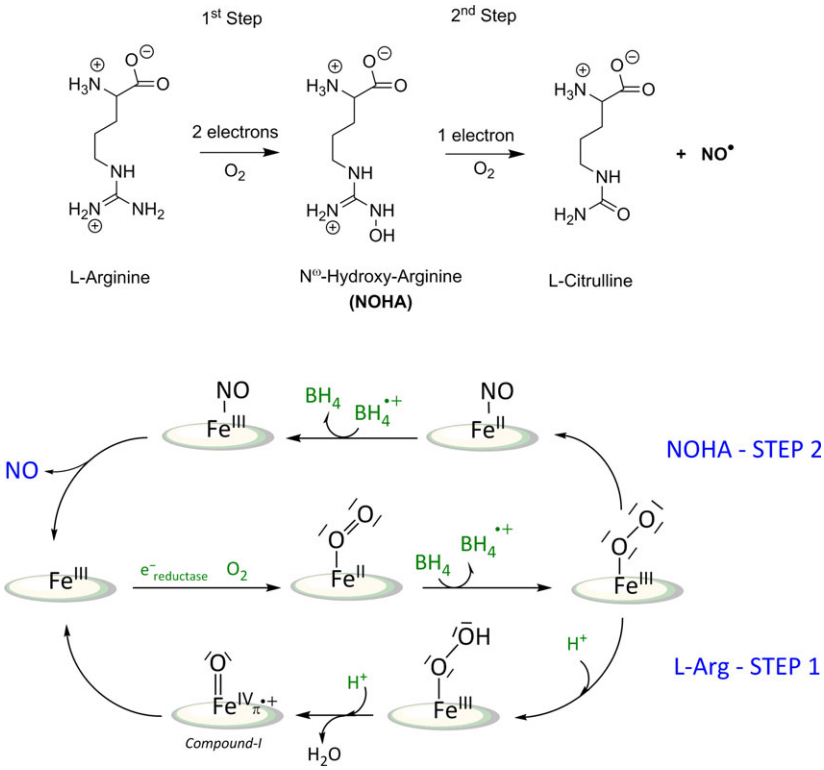

Fig. 1. Catalytic and molecular mechanism of NOS. A: The two oxidative steps that sequentially convert the guanidinium moiety of Arg into NOHA and L-citrulline with NO as side-product. B: Current model of NO-Synthase molecular mechanism. So far, only the initial and final intermediates (Fe^{II}-O_2 and Fe^{III}-NO/Fe^{III}) have been trapped and characterised in catalytic conditions. The key catalytic intermediates (haem-peroxo, oxoferryl and ferrous haem-NO complexes) remain yet to be identified.

the heart of NOS molecular mechanism for it controls the balance between Arg hydroxylation (two protons) and NOHA oxidation (one proton), and tunes the coupling between electron transfer and oxygen activation, preventing NOS uncoupling and ROS production.

There are only few data on proton transfer and no comparative investigation of Steps 1 and 2. This is mostly due to the instability of the Fe^{II}-O_2 intermediate, which requires often the use of noncatalytic conditions (redox analogues, low temperature...). However, some reports have addressed the question of proton transfer and/or the protonation of haem-oxo species [13]: among them, a large series of works have established the influence of the distal environment on the electronic structure, stability and reactivity of Fe^{II}-O_2, -CO and -NO species [29–33]. X-ray and Raman data [29,32,34–36] have clearly shown that the H-bond distal network undergoes a rearrangement as a function of the nature of the substrate (Arg, NOHA, analogues), with changes in the interaction between the substrate guanidinium and the distal ligand and in the role of a vicinal water molecule. We utilised a series of Arg analogues that were distributed along three groups according to their influence on the distal H-bond network as determined from the spectroscopic signature of the CO complex probed with resonance Raman (RR) spectroscopy [33]: Family 1 analogues had an effect similar to that of L-Arg, Family 2 similar to NOHA and Family 3 corresponded to analogues that bind the active site but do not induce a spectroscopic signature, thus mimicking the absence of substrate. We showed that these changes modify the reactivity of the Fe^{II}-O_2 species [33,37] and the fate of the ferric haem-peroxo intermediate: in the presence of Arg, the oxo ligand would be H-bonded to the water molecule, favouring the O-O heterolytic cleavage (and the build-up of a Cpd I-like species), whereas the direct H-bond between NOHA guanidinium and the peroxo species would favour its stability and its direct reactivity [33]. This indicates that the difference between Steps 1 and 2 depends on the structure of the distal H-bond network: the distal water molecule would therefore be required for the first catalytic step (Arg hydroxylation) but not for the second one (NOHA oxidation) [13,33]. This has been confirmed by the work of Marletta and coworkers with 5-methyl Arg and NOHA analogues [38].

This model has been mostly thought of from data using Fe^{II}-O_2 mimics such as the stable Fe^{II}-CO and Fe^{II}-NO complexes. However, these species present structural and electronic properties different from those of Fe^{II}-O_2. To overcome the instability of Fe^{II}-O_2, that prevents its direct investigation, we have used here two complementary fast-kinetics approaches: (a) the stopped-flow set-up coupled to UV–vis spectrometry allows determining the rate constants of O_2 activation and autoxidation; (b) the T-mixer set-up coupled to RR spectroscopy allows characterising the structural properties of Fe^{II}-O_2 intermediate and identifying short-lived intermediates undetected by UV–visible spectroscopy.

We used this approach on one hand to investigate the effect of Arg analogues on the Fe^{II}-O_2 complex and verify the actual role of the water molecule in NOS catalysis, and on the other hand to trap and characterise new reaction intermediates that may intervene in Arg hydroxylation.

Experimental procedures

Chemicals

The synthesis of the hydrochloride salts of *n*-pentyl-guanidine (Pentylgua), 4-fluorophenyl-guanidine (4-Fphgua), 4-chlorophenyl-guanidine (4-Clphgua), 4-trifluoromethyl-phenyl-guanidine (4-CF_3-phgua) and 4-methoxyphenyl-guanidine (4-MeOphgua) (Fig. 2) have been described elsewhere [37]. BH_4 and Arg were purchased from Enzo Life Sciences (Enzo Life Sciences, Farmingdale, NY, USA)

Enzyme preparation

Mouse iNOS oxygenase domain (iNOSoxy) containing a six-histidine tag at its C-terminus was expressed in *Escherichia coli* BL21 using the PCWori vector and purified as already described [39] in the absence of BH_4 and Arg.

Stopped-flow experiments

The protein samples containing BH_4/BH_2 were obtained by preincubation at 4 °C in the presence of 200 μM BH_4/400 μM BH_2 and 5 mM Arg or 10 mM of compounds Pentylgua and 4-Fphgua in 100 mM Kpi buffer (pH 7.4). The binding of the guanidine derivatives and BH_4 was confirmed by measuring the low-spin (420 nm) to the high-spin (395 nm) transition of the haem using UV–vis spectroscopy. The samples were made anaerobic by several cycles of vacuum and argon refilling. The reduction in the haem was achieved by progressive addition of an anaerobic solution of sodium dithionite and followed by monitoring the change in the Soret peak from 395 nm for the ferric form to 412 nm for the ferrous one. The rapid-mixing stopped-flow experiments were performed at 4 °C on a Bio-Logic SFM 300 instrument customised for anaerobic and semianaerobic experiments and connected to a Tidas 1024-diode array detector able of recording spectra every 3 ms. The reduced enzyme was transferred into the stopped-flow

apparatus with a gastight syringe and was rapidly mixed with an equal volume of air saturated buffer. Spectra were recorded between 350 and 700 nm with a total measurement time between 2 and 5 s.

Stopped-flow data analysis

We used a direct examination of the recorded spectra with the absorbance cross sections at specific wavelengths performed with ORIGINPRO 8.0 software (OriginLab Corporation, Northampton, MA, USA). First, visual analysis of the spectra with BH_2 allowed us to identify the different haem species involved in the single-turnover reaction: ferrous Fe^{II} (412 nm), ferrous dioxygen Fe^{II}-O_2 (427–430 nm) and ferric Fe^{III} (395 nm) complexes.

The determination of quantitative transition rates were obtained by combining different methods. The autoxidation rates (in the presence of BH_2) reported by Moreau *et al.* [37] were determined by global analysis (SPECFIT) and by simulation of time traces at 428/395/650 nm to a mono-exponential function. Rate constants obtained by these different methods were similar for every condition [37]. In this report, autoxidation rates were obtained by global analysis like Moreau *et al.* [37] but also by simulation of the 428 nm time trace to a biexponential function. Here again, rates obtained via these two methods were similar.

Activation rates (in the presence of BH_4) were all obtained like Moreau *et al.* [37], that is, by simulation of the 395 nm time traces to a single mono-exponential function, except in the presence of Arg and 4-methoxyphenylguanidine, for which we simulated the kinetics to a biexponential function.

Resonance Raman spectroscopy of iNOSoxy oxygenated intermediates

The buffer used for kinetic measurements was 100 mM KPi, pH 7.4. To prepare the ferrous form of iNOSoxy, the ferric enzyme (80 μM) was equilibrated with nitrogen gas for 30 min at room temperature, and the haem was then reduced with sodium dithionite. Complete reduction in iNOSoxy was verified by optical spectroscopy. Oxygen-containing buffer solutions were prepared by equilibrating deoxygenated buffer with $^{16}O_2$ or $^{18}O_2$. The rapid T-mixer used here was described previously [40]. Oxygen was removed from the mixer with an anaerobic buffer prior to connecting the syringes containing the ferrous protein and oxygen-saturated buffer. The output at 413.1 nm is from a Kr ion laser (Innova 302 Kr; Coherent, Santa Clara, CA, USA) at 10 mW. The output at 441.6 nm is from a He/Cd ion laser (Liconix Laser; Melles-Griot, Ottawa, ON, Canada) at 10 mW. The position of the laser-focusing point was moved along the flow direction to obtain the desired time point. The flow rate was adjusted to result in a time point of 1.25 ms mm^{-1}. The data were measured at time delays after mixing ranging from 4 to 40 ms and measurements were recorded at room temperature (25 °C). The RR spectra were calibrated with the signals from indene. The RR spectrum of reduced myoglobin was recorded prior to each mixing experiment and was used to adjust small differences in the calibration of spectra from different mixing experiments.

Results

Kinetic analysis of Fe^{II}-O_2 activation and autoxidation reactions

We first investigated the effect of Arg and various aryl-guanidines on the kinetics of oxygen activation and of Fe^{II}-O_2 autoxidation. This work aimed at completing the results we previously obtained [33,37] for supplemental compounds of Family 2 and 3 analogues (Fig. 2) in order to determine the best conditions for the T-mixing experiments observed by RR spectroscopy, in particular the optimal build-up times. We used the same stopped-flow methods and the same kinetic analysis [33,37] (see Experimental procedures) to determine the rates of Fe^{II}-O_2 autoxidation in the presence of BH_2 (a redox-inactive BH_4 analogue) and the rates of oxygen activation, in the presence of BH_4.

In the presence of BH_2, we observed the same $Fe^{II} \rightarrow Fe^{II}$-$O_2 \rightarrow Fe^{III}$ transition in the presence of Arg (Fig. 3A) or various aryl-guanidines analogues (Fig. 3B). The rates of Fe^{II}-O_2 decay were determined by simulating the time traces at 427 nm (Fe^{II}-O_2 formation and decay) and at 395 nm (Fe^{III} recovery) with a biexponential function (see Experimental procedures). Our results confirm that changes in the substrate does not modify oxygen-binding rate (k_1) but that autoxidation rates (k_2) successively increase for Family 1 and Family 2/3 analogues, as already described [37] (Fig. 4A, Table 1). In the presence of BH_4, the same sequence of intermediates is observed (Fig. 4B) with a smaller build-up of the Fe^{II}-O_2 species (Fig. 3C,D), illustrating the oxygen activation upon an electron transfer from BH_4, as already reported [41–43]. The kinetics analysis confirms the absence of Fe^{II}-O_2 build-up in the presence of aryl-guanidines analogues, as previously reported [41–43]. The moderate increase in the rate of Fe^{III} recovery (between 12% and 100%, Table 1) should not have prevented observing the build-up of this intermediate (Fig. 4C), suggesting the existence of a transient reaction intermediate that cannot be observed by conventional UV–visible spectrometry, as already proposed [37].

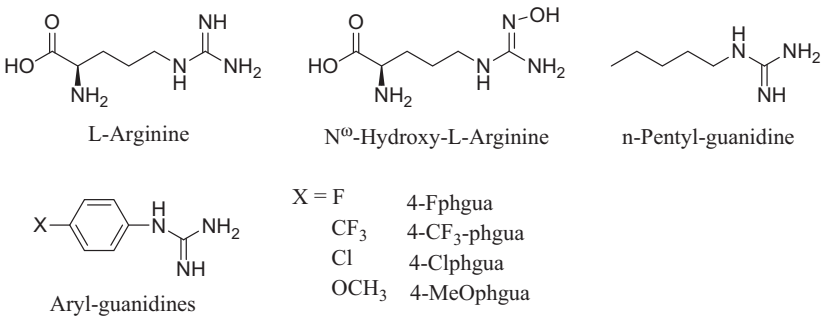

Fig. 2. Structure of *n*-pentylguanidine and aryl-guanidines studied in this work.

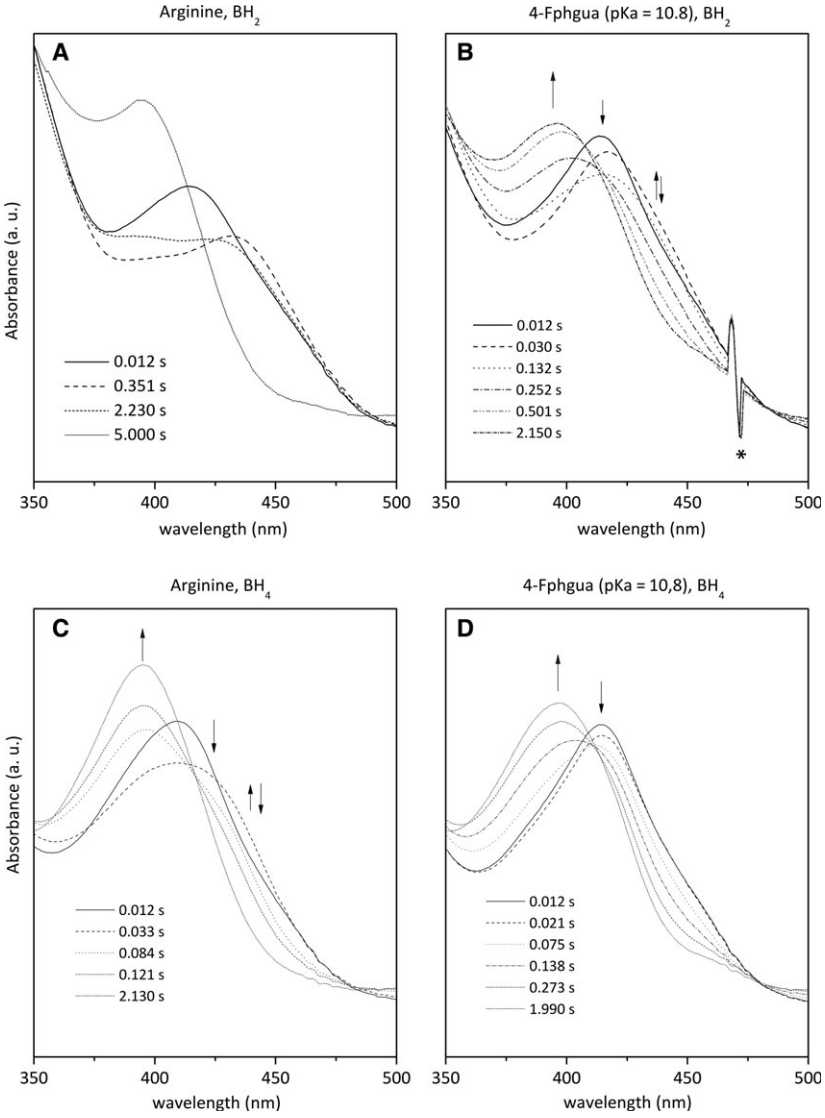

Fig. 3. Absorbance spectra for the reaction of ferrous iNOSoxy with oxygen, in the presence of BH_2 (A, B) or BH_4 (C, D) and L-Arg (A, C) or 4-Fphgua (B, D). The enzyme was rapidly mixed at 4 °C with an equal volume of oxygen-saturated buffer (see Experimental procedures). Solid lines correspond to the spectra of the initial reduced forms; dashed and dotted lines correspond to the spectra at various times after rapid-mixing.

Our results confirm the existence of three families of aryl-guanidine that do not modify binding and coordination of dioxygen to iNOSoxy but that might affect Fe^{II}-O_2 stability [37]. Kinetic analysis of oxygen activation in the presence of BH_4 supports our early hypothesis of the transient formation of an additional reaction intermediate [37]. We then used RR spectroscopy coupled to fast-kinetics methods to directly analyse the effect of aryl-guanidine binding on dioxygen coordination and to look for potential new intermediates.

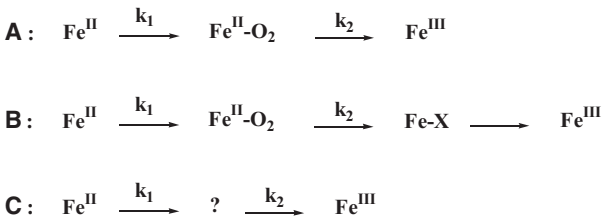

Fig. 4. Reaction sequences analysed by optical stopped-flow spectroscopy and RR spectroscopy with the T-mixer. A: Autoxidation reaction (in the presence of BH_2). Rates between 0.2 and 19 s^{-1} [33,37]. B: Oxygen activation reaction (in the presence of BH_4). Rates of the ferric heme recovery around 20 s^{-1} [33,37]. C: Oxygen activation reaction in the presence of Family 2 analogues. Rates of the ferric heme recovery are smaller than those of Fe^{II}-O_2 build-up [33,37].

Resonance Raman spectroscopy characterisation of NOS mechanism of hydroxylation

The nature of the intermediates formed in the course of Arg and Arg analogues oxidation have been analysed by resonance Raman spectroscopy using a home-built T-mixer set-up [40] (see Experimental procedures). Solutions of reduced iNOSoxy in the presence of Arg or Arg analogues are mixed with $^{16}O_2$- or $^{18}O_2$-saturated buffers and continuously pushed along a 250-μm wide quartz tube. Focusing the RR laser beam at different distances from the mixing point allows determining the vibration modes of all species present in the reaction sample at a defined time (see Experimental procedures). We used two excitation wavelengths (413.1 and 441.6 nm) and recorded a spectral window that covers the 650–1600 cm^{-1} region. We focused on characteristic porphyrin modes and looked for the appearance of new bands that could reflect the O-O stretch modes of Fe^{II}-O_2 or other haem-peroxo or hydroperoxo complexes. We used the kinetics data obtained by stopped-flow to define the time of maximal Fe^{II}-O_2 build-up (see Experimental procedures).

We first look to iNOSoxy-catalysed oxidation of Arg (Fig. 5). The upper spectrum (Fig. 5A) shows the RR fingerprint of the sample for a 10 ms reaction time in the presence of $^{16}O_2$. We observe a mixture of species with a minor fraction of the initial Fe^{II} species (bands ν_4 at 1469 cm^{-1}) and mostly ferric-like complexes with characteristic bands at ν_7 (677 cm^{-1}), ν_5 (1128 cm^{-1}) and ν_4 (1373 cm^{-1}). Most of iNOSoxy seems to have reacted to form a mixture of Fe^{III} and Fe^{II}-O_2 species with characteristic ν_3 bands at 1488 cm^{-1} (Fe^{III}) and 1502 cm^{-1} (Fe^{II}-O_2) [29,32]. The Fe^{II}-O_2 $\nu_{O\text{-}O}$ is difficult to detect for it is expected around 1125 cm^{-1} [32] and is overlapping with the porphyrine mode ν_5 (1122 cm^{-1}). For this reason, we achieved the same experiment with a $^{18}O_2$-saturated buffer that results in an isotopic shift of $\nu_{O\text{-}O}$ down to 1060 cm^{-1} but leaves ν_5 unaffected (Fig. 5B). The difference between the $^{16}O_2$ and the $^{18}O_2$ spectra (Fig. 5C) specifically reveals the Fe^{II}-O_2 $\nu_{O\text{-}O}$ bands but not additional bands from other haem-oxy species. Fitting of the $^{16}O_2/^{18}O_2$ difference spectrum (see Experimental procedures) confirms the frequency of the $\nu_{O\text{-}O}$ mode at 1127 ($^{16}O_2$) and 1060 cm^{-1} ($^{18}O_2$), which is similar to what has been reported previously [32] (Fig. 5 inset; Table 2). We achieved the same experiments using an additional excitation wavelength at 441.6 nm in $^{16}O_2$ and $^{18}O_2$ saturating conditions. We observed the same vibration modes for the Fe^{II}-O_2 intermediate (data not shown) at similar frequencies (Table 2). Whatever the excitation wavelength or the O_2-saturating conditions, we did not observe any new intermediates such as Fe^{III}-OO^- or Fe^{III}-OOH during Arg oxidation reaction, for which the O-O stretching mode would have been observed around 799 ($^{16}O_2$) and 755 ($^{18}O_2$) cm^{-1}, values reported for cytochromes P450 complexes [44].

We repeated the same series of experiments with $^{16}O_2$ and $^{18}O_2$ in the presence of BH_4 and Pentylgua, an Arg analogue from Family 1 [33]. The RR fingerprints of

Table 1. Determination of autoxidation (BH_2) and activation rates (BH_4) in the presence of Arg and various Arg analogues.

		Arg (pKa = 12.5)		Family 1 Pentylgua (pKa = 12.6)		Family 2 4-Fphgua (pKa = 10.8)		Family 2 4-CF_3-phgua (pKa = 10)		Family 2 4-Clphgua (pKa = 10.3)		Family 3 4-MeOphgua (pKa = 11)	
		BH_2	BH_4	BH_2	BH_4	BH_2	BH_4	BH_2	BH_4	BH_2	BH_4	BH_2	BH_4
This report	k_1, s^{-1}	> 50	> 50	nd	nd	24.2	nd	> 50	nd	45	nd	> 50	> 50
	k_2, s^{-1}	0.2	19.0	nd	nd	6.3	7.1	9	18.4	5.9	8.9	11	16.6
[37]	k_1, s^{-1}	> 50	nd	> 50	nd	> 50	nd	nd	nd	> 50	nd	> 50	nd
	k_2, s^{-1}	0.2	20.5	1.9	20.4	12.0	9	nd	nd	7.3	12.3	18.9	31

k_1 values corresponds to oxygen binding rate and k_2 values to FeII-O_2 decay rate. Experiments with 4-CF3-phgua, 4-Clphgua and 4-MeOphgua analogues (not shown) were achieved and analysed with the same protocols as the ones described for 4-Fphgua analogue (See Experimental procedures). nd, not determined.

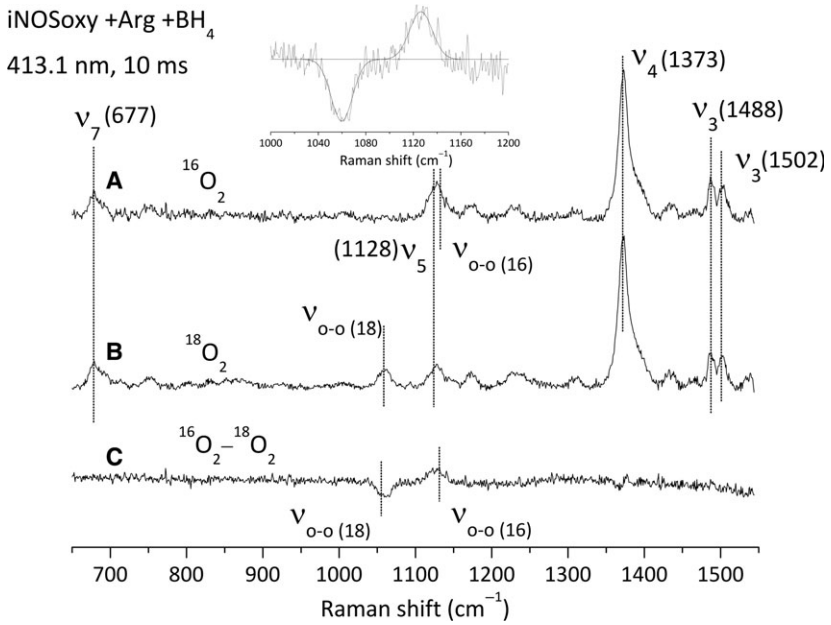

Fig. 5. Resonance Raman spectra recorded at 413.1 nm of the $Fe^{II}O_2$ complex of iNOSoxy in the presence of Arg and BH_4. (A) Resonance Raman spectrum of the $Fe^{II}O_2$ ($^{16}O_2$) complex. (B) Resonance Raman spectrum of the $Fe^{II}O_2$ ($^{18}O_2$) complex. (C) $^{16}O_2$ minus $^{18}O_2$ difference spectrum of $Fe^{II}O_2$ iNOSoxy complex (A minus B). The protein concentration used is about 40 μM after mixing and the spectra are recorded at 10 ms after mixing. Inset: simulation of the 1000–1200 cm^{-1} spectral region by a multigaussian function.

Table 2. Frequencies of the Raman lines of the dioxygen adducts observed with iNOSoxy and L-Arg or Pentylgua or 4-Fphgua.

	λ_{max} (nm)	Time (ms)	$\nu_{o\text{-}o}$ ($^{18}O_2$) (cm^{-1})	$\nu_{o\text{-}o}$ ($^{16}O_2$) (cm^{-1})
Substrate-free [33]	413.1	2	1067	1133
Arg (pKa = 12.5)	413.1	10	1060	1127
Arg	441.6	10	1060	1127
Arg [33]	413.1	2	1060	1126
Pentylgua (pKa = 12.6)	413.1	10	1062	1131
Pentylgua	441.6	40	–	–
Pentylgua	441.6	20	1061	1131
Pentylgua	441.6	4	1061	1130
4-Fphgua (pKa = 10.8)	413.1	10	1064	1130
4-Fphgua	441.6	10	–	–
4-Fphgua	441.6	4	–	–
NOHA (pKa = 8.1) [33]	413.1	2	1066	1132

–, not observed.

the reaction sampled at 10 ms are displayed in Fig. 6. We observed porphyrin modes of the ferric species (Fig. 6, spectra A, B) at 677 cm^{-1} (ν_7), 1122 cm^{-1} (ν_5), 1373 cm^{-1} (ν_4) and 1487 cm^{-1} (ν_3). The ν_3 mode of the Fe^{II}-O_2 intermediate is observed at 1503 cm^{-1}. The $^{16}O_2/^{18}O_2$ difference spectrum shows the $\nu_{O\text{-}O}$ mode in the $^{16}O_2$ and $^{18}O_2$ saturating conditions (Fig. 6, spectrum C). Fitting of the 1000–1200 spectral region (Fig. 6, inset) indicates $\nu_{O\text{-}O}$ frequencies at 1131 ($^{16}O_2$) and 1062 cm^{-1} ($^{18}O_2$). These values are comparable but slightly higher than the ones reported in the presence of Arg. Likewise, the same experiments have been achieved using a 441.6-nm excitation wavelength and at additional reaction times, that is, 4, 20 and 40 ms. We observe a maximum build-up of the Fe^{II}-O_2 intermediate at 4 ms, followed by a decrease in the intensity of the $\nu_{O\text{-}O}$ bands leading to the complete disappearance of the Fe^{II}-O_2 species at 40 ms (data not shown). The frequencies of the $\nu_{O\text{-}O}$ modes are again similar to those determined at 413.1 nm ($\nu_{O\text{-}O(16)}$ = 1130–1131 cm^{-1} and $\nu_{O\text{-}O(18)}$ = 1061–1062 cm^{-1}; Table 2)

The last series of T-mixer/RR experiment was achieved in the presence of BH_4 and 4-Fphgua, an Arg analogue from Family 2 for which no $Fe^{II}O_2$ intermediate has been observed by stopped-flow [33]. We observed the final ferric iNOSoxy modes at 677 cm^{-1} (ν_7), 1122 cm^{-1} (ν_5),1374 cm^{-1} (ν_4) and 1488 cm^{-1} (ν_3) with again a contribution at 1506 cm^{-1} that could be assigned to the ν_3 mode of an $Fe^{II}O_2$ intermediate (Fig. 7, spectra A, B). The $^{16}O_2/^{18}O_2$ difference spectrum (Fig. 7, spectrum C) reveals the presence of $\nu_{O\text{-}O}$ vibrational mode in both the $^{16}O_2$ and $^{18}O_2$ conditions. The fitting of the 1000–1200 spectral region (Fig. 7, inset) leads to $\nu_{O\text{-}O}$ frequencies at 1130 ($^{16}O_2$) and 1064 cm^{-1} ($^{18}O_2$). Unexpectedly, these modes were not observed using an excitation wavelength at 441.6 nm and did not allow either to identify other haem-oxy intermediates (data not shown).

Discussion

The characteristics of proton transfer process are a major topic to understand the mechanism of oxygen activation by NOS. Using a series of synthetic analogues of Arg, we recently proposed a model with the distal water molecule as potential second proton donor [33]. The H-bond established between this water molecule

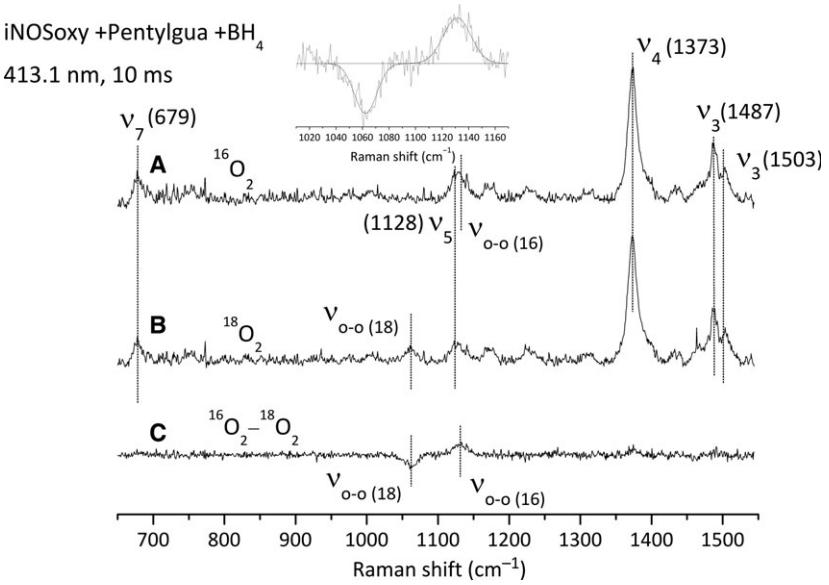

Fig. 6. Resonance Raman spectra recorded at 413.1 nm of the $Fe^{II}O_2$ complex of iNOSoxy in the presence of Pentylgua and BH_4. (A) Resonance Raman spectrum of the $Fe^{II}O_2$ ($^{16}O_2$) complex. (B) Resonance Raman spectrum of the $Fe^{II}O_2$ ($^{18}O_2$) complex. (C) $^{16}O_2$ minus $^{18}O_2$ difference spectrum of $Fe^{II}O_2$ iNOSoxy complex (A minus B). The protein concentration used is about 40 μM after mixing and the spectra are recorded at 10 ms after mixing. Inset: simulation of the 1010–1170 cm^{-1} spectral region by a multigaussian function.

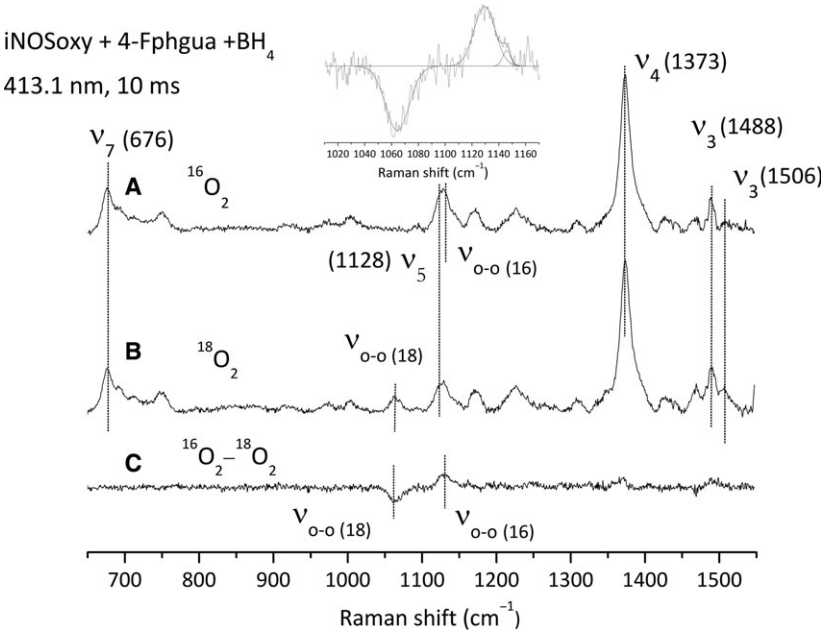

Fig. 7. Resonance Raman spectra recorded at 413.1 nm of the $Fe^{II}O_2$ complex of iNOSoxy in the presence of 4-Fphgua and BH_4. (A) Resonance Raman spectrum of the $Fe^{II}O_2$ ($^{16}O_2$) complex. (B) Resonance Raman spectrum of the $Fe^{II}O_2$ ($^{18}O_2$) complex. (C) $^{16}O_2$ minus $^{18}O_2$ difference spectrum of $Fe^{II}O_2$ iNOSoxy complex (A minus B). The protein concentration used is about 40 μM after mixing and the spectra are recorded at 10 ms after mixing. Inset: simulation of the 1010–1170 cm^{-1} spectral region by a multigaussian function.

and the dioxygen ligand would be stabilized in the presence of Arg, but not NOHA. Thus, the nature of the distal H-bond network appears as a key element in tuning ferric haem-superoxo/peroxo reactivity and as such might control the balance between heterolytic cleavage (Step 1) and nucleophilic attack (Step 2) [13,33,36].

A new approach to investigate oxygen activation mechanism

In this work, we wished to extend the model we deduced from the analysis of the structure of the Fe^{II}-CO complex [33] to the relevant Fe^{II}-O_2 intermediate and establish a direct correlation between Fe^{II}-O_2 structure/reactivity and its interaction with the distal H-bond network. Following our first hypotheses [37], we aimed at identifying potential new haem-oxy intermediates formed in the course of aryl-guanidines oxidation. For this matter, we chose to combine the use of synthesised Arg analogues to an alternative and efficient fast-kinetic approach, a T-mixer device coupled to RR spectroscopy [40]. Continuous flow analysis allows recording RR spectra for reaction times as small as a millisecond. These short-time recordings

might allow identifying short-lived intermediates such as the Fe^{II}-O_2 complex in the presence of Arg analogues. Besides, resonance Raman is an appropriate spectroscopy for characterising Fe^{II}-O_2 structural properties and for identifying species that cannot be observed by UV–visible spectroscopy. We first furthered our initial stopped-flow experiments in order to complete the set of kinetic parameters for single-turnover oxidation reactions for various analogues of Arg (Table 1). Monitoring the absorbance at 428 nm during stopped-flow analyses allows the estimation of the Fe^{II}-O_2 build-up and decay kinetics for the various oxidation reactions. It provides kinetic information that is essential to the trapping of reaction intermediates. We used two distinct excitation wavelengths (413.1 and 441.6 nm) to optimise the excitation and to reveal intermediates that exhibit different absorption profiles by RR spectroscopy. The frequencies determined for the porphyrin and $\nu_{O\text{-}O}$ modes are independent from the excitation wavelength. The RR fingerprint of the reaction sampled regularly shows a mixture between the initial ferrous species, the final ferric species and the Fe^{II}-O_2 intermediate which suggests that the chosen analysis time corresponds to the very middle of the reaction and is appropriate to trap Fe^{II}-O_2 or any other haem-oxy intermediates. We also analysed the reaction mixture at different times (4, 10, 20, 40 ms). We observed that all RR spectra showed the presence of the Fe^{II}-O_2 species with an apparent maximum build-up around 4 ms and a complete decay at 40 ms, which validates the choice of a reaction time at 10 ms. The method we set up proved to be appropriate since we were able to trap and characterise the Fe^{II}-O_2 intermediate in the presence of aryl-guanidines, which was not possible by UV–Visible absorption spectroscopy. The characterisation of the vibration modes of the Fe^{II}-O_2 complex allowed us to investigate the interaction of Fe^{II}-O_2 intermediate with its distal environment, and more particularly the H-bond between the water molecule and the O_2 distal ligand.

We determined the frequencies of the $\nu_{O\text{-}O}$ modes of the Fe^{II}-O_2 intermediate in the presence of Arg, pentylguanidine (Family 1) and 4-Fphgua (Family 2). Frequencies are reported in Table 1 and show variations in the frequencies of the $\nu_{O\text{-}O}$ mode as a function of the substrate bound in the pocket. The proximity between the frequencies of the $\nu_{O\text{-}O}$ and the porphyrin ν_5 modes could lead to a vibrational coupling between these vibrations. This coupling would correspond to a degeneration of the $\nu_{O\text{-}O}$ and ν_5 modes that would induce an enhancement of the porphyrin ν_5 intensity and a shift of the $\nu_{O\text{-}O}$ frequency towards ν_5 frequency [45]. For this reason, comparison among the analogues and substrates are discussed based on the $^{18}O_2$ frequencies. In the presence of Pentylgua, the $\nu_{O\text{-}O}$ frequency increases by 1–2 cm^{-1} (2–4 cm^{-1} in $^{16}O_2$ conditions), which is reminiscent to what has been observed for the $\nu_{C\text{-}O}$ mode of the Fe^{II}-CO complex [33], suggesting a weakening of the H-bond between the water molecule and the dioxygen ligand. Although the arginine → Pentylgua substitution preserves the structure of the H-bond (and the H-bonding with the water molecule) changes in the guanidine structure might lead to a small destabilisation and weakening of this H-bond, which is illustrated by the increased Fe^{II}-O_2 autoxidation rate in the presence of Pentylgua. On the other hand, the Arg analogues from Family 2 are believed to modify the H-bond distal network in a way similar to that observed for NOHA, that is, by displacing the water molecule away [33]. This led to a strengthening of Fe^{II}-CO $\nu_{C\text{-}O}$ stretch [33] (with respect to the absence of substrate), and likewise should induce an increase in $\nu_{O\text{-}O}$ frequency toward values similar to the substrate-free protein. Indeed, the $\nu_{O\text{-}O}$ frequency increases by 6 cm^{-1} in the presence of NOHA (compared to Arg, Table 2). The same effect is observed in the presence of 4-Fphgua, an aryl-guanidine from Arg analogue Family 2, with an increase in 4 cm^{-1} of the $\nu_{O\text{-}O}$ frequency. This supports our hypothesis concerning the effect of aryl-guanidines on the distal H-bond network: the pKa of these aryl-guanidines (Family 2: 4-Fphgua, 4-CF_3-phgua, and 4-Clphgua) is weaker than that of L-Arg [33]. This gives to the guanidinium proton a more acidic character, which in turn modifies the H-bond network in such a way that the water molecule does not interact anymore with the ligand bound to the haem iron.

Our results show that despite its more linear coordination, CO remains a relatively good mimic of O_2 to investigate O_2 interactions with distal residues and reactivity. Globally, our results confirmed the correlation between the evolution of the vibration modes of the CO and O_2 ligands that sense the changes in the distal environment and in the intensity of the electron back-donation from iron orbitals. The role of NOS substrate in the proton transfer pathway and the nature of proton donor remains a matter of debate. Various reports from the groups of Rousseau [32], Crane [36], Marletta [38], Poulos [35] and from our groups [33,37] support a model of NOS-catalysed oxygen activation in which neither Arg nor NOHA directly act as the second proton donor. Instead, Arg would stabilise the distal H-bond network in which the water plays a crucial role in the proton transfer sequence and in the formation of the oxoferryl intermediate (Step 1). In the presence of NOHA, the removal of the water

molecule and the H-bond between the distal oxygen and the substrate guanidinium stabilises the peroxo intermediate and prevents the Cpd I formation.

Looking for new reaction intermediates

The second axis of our project was to look for reaction intermediates in NOS-catalysed oxygen activation, using the T-mixer/RR set-up to reveal new species, in particular ferric haem-peroxide that could not have been observed by UV–visible absorption spectroscopy. The initial hypothesis rose from the absence of Fe^{II}-O_2 intermediate build-up in the presence of BH_4 and Family 2 aryl-guanidines [37]. This was in opposition with the observation of Fe^{II}-O_2 build-up, (a) in the presence of BH_2 and (b) in the presence of BH_4 and Family 3 analogues, both conditions for which no electron transfer is achieved [37]. This suggests that Family 2 aryl-guanidines do not prevent O_2 binding. The fast Fe^{II}-O_2 build-up opposed to the slow Fe^{III} recovery, suggests the existence of an additional fast step converting Fe^{II}-O_2 into an unknown intermediate that would slowly decay into the final Fe^{III} species (Fig. 4C). Since we were not able to identify this intermediate by stopped-flow, we used the T-Mixer/RR setup to trap and characterise it.

We were able to observe the Fe^{II}-O_2 species in (almost) all conditions. We did not detect additional porphyrin or $\nu_{O\text{-}O}$ bands, which suggested the absence of additional haem intermediate in the presence of Arg and Pentylgua (Family 1), but also with 4-Fphgua, for which we previously hypothesised the transient formation of a haem-peroxide complex. The nonobservation of bands specific to haem-peroxide complex in the crowded 750–800 cm^{-1} spectral region might, however, be due to a weak build-up of these intermediates (that would rapidly decompose into ferric species) and to the weak amplitude of their $\nu_{O\text{-}O}$ bands.

The question of the absence of Fe^{II}-O_2 build-up in stopped-flow experiment remains, leading to two alternative hypotheses: (a) the absorbance of iNOSoxy in the presence of BH_4 and 4-Fphgua might be blue-shifted with an absorption maximum around 420 nm, such as what has been described for Oxy 1 species, a CYP-like ferrous haem-oxo species [30,31]. This is supported by the absence of RR exaltation of the Fe^{II}-O_2 modes using an excitation wavelength at 441.6 nm, which also suggest a blue-shift of Fe^{II}-O_2 absorption. This shift would make the detection of Fe^{II}-O_2 more difficult by optical absorption spectroscopy due to an absorption maximum too close to the Fe^{II} and Fe^{III} species. However, the BH_2/4-Fphgua Fe^{II}-O_2 species displays a maximum absorption around 428 nm, and Family 3 aryl-guanidines do not seem to modify this spectroscopic fingerprint. (b) The intermediate is not a haem-oxy but a low-spin ferric species with an absorption maximum around 415–420 nm. This intermediate could correspond to the produced hydroxy-aryl-guanidine that would be formed rapidly but would remain O-bound to the haem iron [46,47], which resulted in a Low-Spin signature. It would be released slowly, with a rate corresponding to the ferric Low-Spin/High-Spin transition (Fig. 4B). However, our T-Mixer/RR experiments did not show any low-spin signals (apart from that assigned to Fe^{II}-O_2) that could suggest the presence of such a Fe^{III} LS intermediate but instead reported the formation of a Fe^{II}-O_2 species. At this stage, further experiments at longer reaction times are needed to favour any of these hypotheses.

Conclusion

In this work we combined the organic synthesis of tailored substrate analogues with a fast-kinetic approach that coupled a T-Mixer module to resonance Raman spectroscopy: the T-mixer allows investigating of short reaction times and RR is an alternative to optical spectroscopy for deciphering the nature of transient intermediates species. The experiments presented here allowed us to complete the structural characterisation of the Fe^{II}-O_2 intermediate in the presence of various aryl- and alkyl-substrate analogues. However, this advanced approach failed in identifying new intermediates in the oxygen activation reaction of NO-Synthases. The peculiar absence of Fe^{II}-O_2 build-up in the presence of various aryl-guanidines Arg analogues by optical spectroscopy remains unexplained so far and the proposed ferric haem-peroxide species elude any characterisation. Nonetheless, our results confirm the role of the H-bond network, in particular the acidity of the guanidinium and the interaction with the vicinal water molecule. This strengthens the scheme proposed for proton donation [13] that explains the difference between the first catalytic step (the water molecule allows the transfer of two protons and the formation of a $[Fe^{III}\text{-}OOH_2]^+$ intermediate) and the second catalytic step (no water molecule, one proton transfer leading to a Fe^{III}-OOH intermediate). This supports the model proposed for NOS molecular mechanism, for which Arg hydroxylation is related to the heterolytic cleavage of the $[Fe^{III}O\text{-}OH_2]^+$ bond and the build-up of a Cpd I species unlike NOHA oxidation for which the Fe^{III}-OOH species is the oxidative intermediate.

Acknowledgements

The project was supported in part by the French Infrastructure for Integrated Structural Biology (FRISBI) ANR-10-INSB-05-01 and the CNRS PEPII Program. AB acknowledges the CEA for her PhD fellowship (Irtelis program). We thank Sébastien P. Blais for the T-Mixer set-up Scheme in the Graphical Abstract.

Author contributions

JS and MC planned experiments; AB, JL, JS and MC performed experiments; AB, JL, MC, JS analysed data; JLB contributed the analogues; AB, JL, PD, MC, JLB and JS wrote the paper.

References

1 Sessa WC (2004) eNOS at a glance. *J Cell Sci* **117**, 2427–2429.
2 Mungrue IN and Bredt DS (2004) nNOS at a glance: implications for brain and brawn. *J Cell Sci* **117**, 2627–2629.
3 Lowenstein CJ and Padalko E (2004) iNOS (NOS2) at a glance. *J Cell Sci* **117**, 2865–2867.
4 Pacher P, Beckman JS and Liaudet L (2007) Nitric oxide and peroxynitrite in health and disease. *Physiol Rev* **87**, 315–424.
5 Szabo C, Ischiropoulos H and Radi R (2007) Peroxynitrite: biochemistry, pathophysiology and development of therapeutics. *Nat Rev Drug Discov* **6**, 662–680.
6 Halliwell B, Zhao K and Whiteman M (1999) Nitric oxide and peroxynitrite. The ugly, the uglier and the not so good: a personal view of recent controversies. *Free Radical Res* **31**, 651–669.
7 Ischiropoulos H and Gow A (2005) Pathophysiological functions of nitric oxide-mediated protein modifications. *Toxicology* **208**, 299–303.
8 Alderton WK, Cooper CE and Knowles RG (2001) Nitric oxide synthases: structure, function and inhibition. *Biochem J* **357**, 593–615.
9 Li H and Poulos TL (2005) Structure-function studies on nitric oxide synthases. *J Inorg Biochem* **99**, 293–305.
10 Stuehr DJ, Santolini J, Wang ZQ, Wei CC and Adak S (2004) Update on mechanism and catalytic regulation in the NO synthases. *J Biol Chem* **279**, 36167–36170.
11 Roman LJ, Martasek P and Masters BS (2002) Intrinsic and extrinsic modulation of nitric oxide synthase activity. *Chem Rev* **102**, 1179–1190.
12 Stuehr DJ, Tejero J and Haque MM (2009) Structural and mechanistic aspects of flavoproteins: electron transfer through the nitric oxide synthase flavoprotein domain. *FEBS J* **276**, 3959–3974.
13 Santolini J (2011) The molecular mechanism of mammalian NO-synthases: a story of electrons and protons. *J Inorg Biochem* **105**, 127–141.
14 Couture M, Stuehr DJ and Rousseau DL (2000) The ferrous dioxygen complex of the oxygenase domain of neuronal nitric-oxide synthase. *J Biol Chem* **275**, 3201–3205.
15 Wei CC, Crane BR and Stuehr DJ (2003) Tetrahydrobiopterin radical enzymology. *Chem Rev* **103**, 2365–2383.
16 Stuehr DJ, Wei CC, Wang Z and Hille R (2005) Exploring the redox reactions between heme and tetrahydrobiopterin in the nitric oxide synthases. *Dalton Trans* **21**, 3427–3435.
17 Hurshman AR, Krebs C, Edmondson DE, Huynh BH and Marletta MA (1999) Formation of a pterin radical in the reaction of the heme domain of inducible nitric oxide synthase with oxygen. *Biochemistry* **38**, 15689–15696.
18 Bec N, Gorren AC, Voelker C, Mayer B and Lange R (1998) Reaction of neuronal nitric-oxide synthase with oxygen at low temperature. Evidence for reductive activation of the oxy-ferrous complex by tetrahydrobiopterin. *J Biol Chem* **273**, 13502–13508.
19 Wei CC, Wang ZQ, Tejero J, Yang YP, Hemann C, Hille R and Stuehr DJ (2008) Catalytic reduction of a tetrahydrobiopterin radical within nitric-oxide synthase. *J Biol Chem* **283**, 11734–11742.
20 Wei CC, Wang ZQ, Hemann C, Hille R and Stuehr DJ (2003) A tetrahydrobiopterin radical forms and then becomes reduced during Nomega-hydroxyarginine oxidation by nitric-oxide synthase. *J Biol Chem* **278**, 46668–46673.
21 Davydov R, Sudhamsu J, Lees NS, Crane BR and Hoffman BM (2009) EPR and ENDOR characterization of the reactive intermediates in the generation of NO by cryoreduced oxy-nitric oxide synthase from *Geobacillus stearothermophilus*. *J Am Chem Soc* **131**, 14493–14507.
22 Davydov R, Labby KJ, Chobot SE, Lukoyanov DA, Crane BR, Silverman RB and Hoffman BM (2014) Enzymatic and cryoreduction EPR studies of the hydroxylation of methylated N(omega)-hydroxy-l-arginine analogues by nitric oxide synthase from *Geobacillus stearothermophilus*. *Biochemistry* **53**, 6511–6519.
23 Brunel A, Santolini J and Dorlet P (2012) Electron paramagnetic resonance characterization of tetrahydrobiopterin radical formation in bacterial nitric oxide synthase compared to mammalian nitric oxide synthase. *Biophys J* **103**, 109–117.
24 Stoll S, NejatyJahromy Y, Woodward JJ, Ozarowski A, Marletta MA and Britt RD (2010) Nitric oxide synthase stabilizes the tetrahydrobiopterin cofactor radical by controlling its protonation state. *J Am Chem Soc* **132**, 11812–11823.

25 Wei CC, Wang ZQ, Wang Q, Meade AL, Hemann C, Hille R and Stuehr DJ (2001) Rapid kinetic studies link tetrahydrobiopterin radical formation to heme-dioxy reduction and arginine hydroxylation in inducible nitric-oxide synthase. *J Biol Chem* **276**, 315–319.
26 Hannibal L, Somasundaram R, Tejero J, Wilson A and Stuehr DJ (2011) Influence of heme-thiolate in shaping the catalytic properties of a bacterial nitric-oxide synthase. *J Biol Chem* **286**, 39224–39235.
27 Brunel A, Wilson A, Henry L, Dorlet P and Santolini J (2011) The proximal hydrogen bond network modulates *Bacillus subtilis* nitric-oxide synthase electronic and structural properties. *J Biol Chem* **286**, 11997–12005.
28 Lang J, Santolini J and Couture M (2011) The conserved Trp-Cys hydrogen bond dampens the "push effect" of the heme cysteinate proximal ligand during the first catalytic cycle of nitric oxide synthase. *Biochemistry* **50**, 10069–10081.
29 Chartier FJ and Couture M (2007) Substrate-specific interactions with the heme-bound oxygen molecule of nitric-oxide synthase. *J Biol Chem* **282**, 20877–20886.
30 Marchal S, Gorren AC, Sorlie M, Andersson KK, Mayer B and Lange R (2004) Evidence of two distinct oxygen complexes of reduced endothelial nitric oxide synthase. *J Biol Chem* **279**, 19824–19831.
31 Marchal S, Gorren AC, Andersson KK and Lange R (2005) Hunting oxygen complexes of nitric oxide synthase at low temperature and high pressure. *Biochem Biophys Res Commun* **338**, 529–535.
32 Li D, Kabir M, Stuehr DJ, Rousseau DL and Yeh SR (2007) Substrate- and isoform-specific dioxygen complexes of nitric oxide synthase. *J Am Chem Soc* **129**, 6943–6951.
33 Giroud C, Moreau M, Mattioli TA, Balland V, Boucher JL, Xu-Li Y, Stuehr DJ and Santolini J (2010) Role of arginine guanidinium moiety in nitric-oxide synthase mechanism of oxygen activation. *J Biol Chem* **285**, 7233–7245.
34 Li H, Igarashi J, Jamal J, Yang W and Poulos TL (2006) Structural studies of constitutive nitric oxide synthases with diatomic ligands bound. *J Biol Inorg Chem* **11**, 753–768.
35 Doukov T, Li H, Soltis M and Poulos TL (2009) Single crystal structural and absorption spectral characterizations of nitric oxide synthase complexed with N(omega)-hydroxy-L-arginine and diatomic ligands. *Biochemistry* **48**, 10246–10254.
36 Pant K and Crane BR (2006) Nitrosyl-heme structures of *Bacillus subtilis* nitric oxide synthase have implications for understanding substrate oxidation. *Biochemistry* **45**, 2537–2544.
37 Moreau M, Boucher JL, Mattioli TA, Stuehr DJ, Mansuy D and Santolini J (2006) Differential effects of alkyl- and arylguanidines on the stability and reactivity of inducible NOS heme-dioxygen complexes. *Biochemistry* **45**, 3988–3999.
38 Martin NI, Woodward JJ, Winter MB, Beeson WT and Marletta MA (2007) Design and synthesis of C5 methylated L-arginine analogues as active site probes for nitric oxide synthase. *J Am Chem Soc* **129**, 12563–12570.
39 Gachhui R, Ghosh DK, Wu C, Parkinson J, Crane BR and Stuehr DJ (1997) Mutagenesis of acidic residues in the oxygenase domain of inducible nitric-oxide synthase identifies a glutamate involved in arginine binding. *Biochemistry* **36**, 5097–5103.
40 Chartier FJ, Blais SP and Couture M (2006) A weak Fe-O bond in the oxygenated complex of the nitric-oxide synthase of *Staphylococcus aureus*. *J Biol Chem* **281**, 9953–9962.
41 Boggs S, Huang L and Stuehr DJ (2000) Formation and reactions of the heme-dioxygen intermediate in the first and second steps of nitric oxide synthesis as studied by stopped-flow spectroscopy under single-turnover conditions. *Biochemistry* **39**, 2332–2339.
42 Abu-Soud HM, Gachhui R, Raushel FM and Stuehr DJ (1997) The ferrous-dioxy complex of neuronal nitric oxide synthase. Divergent effects of L-arginine and tetrahydrobiopterin on its stability. *J Biol Chem* **272**, 17349–17353.
43 Stuehr DJ, Wei CC, Santolini J, Wang Z, Aoyagi M and Getzoff ED (2004) Radical reactions of nitric oxide synthases. *Biochem Soc Symp* **71**, 39–49.
44 Mak PJ, Denisov IG, Victoria D, Makris TM, Deng T, Sligar SG and Kincaid JR (2007) Resonance Raman detection of the hydroperoxo intermediate in the cytochrome P450 enzymatic cycle. *J Am Chem Soc* **129**, 6382–6383.
45 Wang J, Stuehr DJ and Rousseau DL (1997) Interactions between substrate analogues and heme ligands in nitric oxide synthase. *Biochemistry* **36**, 4595–4606.
46 Lefevre-Groboillot D, Frapart Y, Desbois A, Zimmermann JL, Boucher JL, Gorren AC, Mayer B, Stuehr DJ and Mansuy D (2003) Two modes of binding of N-hydroxyguanidines to NO synthases: first evidence for the formation of iron-N-hydroxyguanidine complexes and key role of tetrahydrobiopterin in determining the binding mode. *Biochemistry* **42**, 3858–3867.
47 Sabat J, Egawa T, Lu C, Stuehr DJ, Gerfen GJ, Rousseau DL and Yeh SR (2013) Catalytic intermediates of inducible nitric-oxide synthase stabilized by the W188H mutation. *J Biol Chem* **288**, 6095–6106.